Role of electric charge in shaping equilibrium configurations of fluid tori encircling black holes

Jiří Kovář,* Petr Slaný, and Zdeněk Stuchlík
Institute of Physics, Faculty of Philosophy and Science, Silesian University in Opava
Bezručovo nám. 13, CZ-74601 Opava, Czech Republic

Vladimír Karas
Astronomical Institute, Academy of Sciences, Boční II, CZ-14131 Prague, Czech Republic

Claudio Cremaschini
SISSA & INFN, Via Bonomea 265, I-34136 Trieste, Italy

John C. Miller
SISSA & INFN, Via Bonomea 265, I-34136 Trieste, Italy and
Department of Physics (Astrophysics), University of Oxford
Keble Road, Oxford OX1 3RH, U.K.

Astrophysical fluids may acquire non-zero electrical charge because of strong irradiation or charge separation in a magnetic field. In this case, electromagnetic and gravitational forces may act together and produce new equilibrium configurations, which are different from the uncharged ones. Following our previous studies of charged test particles and uncharged perfect fluid tori encircling compact objects, we introduce here a simple test model of a charged perfect fluid torus in strong gravitational and electromagnetic fields. In contrast to ideal magnetohydrodynamic models, we consider here the opposite limit of negligible conductivity, where the charges are tied completely to the moving matter. This is an extreme limiting case which can provide a useful reference against which to compare subsequent more complicated astrophysically-motivated calculations. To clearly demonstrate the features of our model, we construct three-dimensional axisymmetric charged toroidal configurations around Reissner-Nordström black holes and compare them with equivalent configurations of electrically neutral tori.

I. INTRODUCTION

Equilibrium toroidal configurations of perfect fluid play an important role in studies of geometrically thick accretion discs around compact objects [1]. The isobaric surfaces also have toroidal topology and in order for accretion to occur there must be a critical, marginally-closed isobaric surface with a cusp through which matter can outflow from the disc onto the compact object. In the following, we focus on black-hole systems and ignore self-gravity of the disc material. Shapes and properties of the tori, such as pressure and density profiles, are then determined by the black-hole spacetime geometry, an appropriately chosen rotation law (giving the distribution of specific angular momentum), and the fluid parameters.

Perfect fluid tori in Schwarzschild and Kerr backgrounds were extensively discussed in the original fundamental papers establishing this line of work [2, 3]. Later on, many studies appeared generalizing these models and including further details [4–10], describing tori also in Schwarzschild-de Sitter, Kerr-de Sitter and Reissner-Nordström-de Sitter spacetimes, where presence of the so-called static radius [11] implies also the existence of tori with an outer cusp.

The material in accretion discs contains charged particles (which may or may not be quasi-neutral in bulk) and the central black hole might also be charged. The charged or quasi-neutral fluid creates its own electromagnetic field which would then couple with that of the black hole, leading to a different and much more complicated description of the motion. Using the equations for the dynamics of the fluid and specifying its 'internal' properties (conductivity, viscosity, equation of state, etc), one can solve the system so as to obtain profiles for the four-velocity, pressure, matter density and charge density [12]. However, the system of equations is rather complex, and in general requires the use of sophisticated numerical approaches and codes, even if simplifying assumptions are made such as taking infinite electrical conductivity (the limit of 'ideal magnetohydrodynamics'), no self-gravity, etc. On the other hand, some characteristic features of the motion of quasi-neutral or charged fluid, can also be studied relatively simply in a semi-analytic way [13–20].

The approximation of ideal magnetohydrodynamics (MHD) is reasonable in many astrophysically-relevant situations involving fluids in motion [21]. However, there are other physical circumstances in which it is important to include the effects of finite conductivity [22–24], and there the behavior becomes more complex, especially when strong gravitational and external magnetic fields are also present. In order to address some of these effects in their mutual interplay, it can be useful to look also

*Electronic address: Jiri.Kovar@fpf.slu.cz

at the opposite limit to that of ideal MHD: the limit of negligibly small conductivity.

Here, we examine the problem of the interaction between charged moving matter and the gravitational and electrostatic fields of the black hole, concentrating on an idealized situation which allows us to illustrate some otherwise very complicated effects. We consider a simple test model in which the matter is taken to be slightly charged and electrically non-conductive (dielectric), with the aim of providing an extreme reference case against which to compare subsequent more detailed calculations. We proceed by first specifying a prescribed form for the angular momentum distribution, and then solving the dynamical equations to find the profiles of pressure, mass density and charge density. This approach can be seen as generalizing the studies of uncharged perfect-fluid tori mentioned above by adding the charge. Note that, throughout, our tori are assumed to be composed of test fluids in which both the self-gravitational and self-electromagnetic fields are neglected. This gives a useful simplification, which is acceptable for weakly-charged, low-mass tori that have hardly any effect on the spacetime geometry or the ambient electromagnetic field. This approach helps us in building a semi-analytic model. In principle, inclusion of self-gravity of the tori (following, e.g. [25–27]) and self-electromagnetic effects (see, e.g. [16]) would be possible, but that would enormously complicate the situation.

The charged dielectric perfect-fluid tori can also be seen as generalizing studies of charged test particles orbiting around black holes [28–36]. Various aspects of the charged test particle motion were also discussed in [37, 38], concerning the possibility of collimated ejection along the axis of a rotating magnetized black hole, while investigation of stable off-equatorial lobes of charged particles was discussed in [39–41]. In general, the motion of test particles is bounded within effective potential wells and this represents a model for a very dilute toroidal structure consisting of non-interacting particles; here, we add the non-electrical interaction between them, the pressure. Commonly, pressure leads to geometrically thick structures extending further out of the equatorial plane.

In section II, we present the basic equations. In section III, we apply them to the case of a torus around a charged, non-rotating black hole described by the Reissner-Nordström metric. Nevertheless, the presented approach is suitable for a description of charged tori near to any models of compact objects with well-defined geometry and electromagnetic field. We chose the Reissner-Nordström black hole because of its extremely clear external electric field and geometry, given in an analytic form. For illustrative purposes we set the charge of the central black hole considerably exceeding astrophysically realistic values; our paper presents a toy model exhibiting the physical mechanism of mutual interaction between charged fluid and a black hole. In section IV, we discuss the form of the isobaric surfaces for a torus with constant specific angular momentum composed of an uncharged barotropic perfect fluid. This is then extended to charged tori in section V, where we also present a comparison between equivalent charged and uncharged cases. This work involves making a number of simplifying assumptions, and we discuss the nature and impact of these (including the zero-conductivity limit) in section VI. Section VII is the conclusion. Throughout the paper, we use the geometrical system of units ($c = G = 1$) and metric signature +2.

II. BASIC EQUATIONS

In general, the motion of charged perfect fluid is described by two sets of general relativistic MHD equations. These are the conservation laws and Maxwell's equations

$$\nabla_\beta T^{\alpha\beta} = 0, \tag{1}$$

$$\nabla_\beta F^{\alpha\beta} = 4\pi J^\alpha, \tag{2}$$

where the 4-current density J^α, which satisfies the continuity equation

$$\nabla_\alpha J^\alpha = 0, \tag{3}$$

can be expressed in terms of the charge density q, conductivity σ and 4-velocity U^α of the fluid by using Ohm's law

$$J^\alpha = qU^\alpha + \sigma F^{\alpha\beta}U_\beta, \tag{4}$$

with the electromagnetic tensor $F^{\alpha\beta}$ being given in terms of the vector potential by $F_{\alpha\beta} = \nabla_\alpha A_\beta - \nabla_\beta A_\alpha$. This electromagnetic tensor describes the vacuum external electromagnetic field of the compact object (which pervades the fluid), and also the internal electromagnetic field of the fluid itself, i.e.,

$$F^{\alpha\beta} = F^{\alpha\beta}_{\rm EXT} + F^{\alpha\beta}_{\rm INT}. \tag{5}$$

The stress-energy tensor $T^{\alpha\beta}$ consists of matter and electromagnetic parts

$$T^{\alpha\beta} = T^{\alpha\beta}_{\rm MAT} + T^{\alpha\beta}_{\rm EM}, \tag{6}$$

where

$$T^{\alpha\beta}_{\rm MAT} = (\epsilon + p)U^\alpha U^\beta + pg^{\alpha\beta}, \tag{7}$$

$$T^{\alpha\beta}_{\rm EM} = \frac{1}{4\pi}\left(F^\alpha{}_\gamma F^{\beta\gamma} - \frac{1}{4}F_{\gamma\delta}F^{\gamma\delta}g^{\alpha\beta}\right). \tag{8}$$

Besides the pressure p and energy density ϵ, the other fluid variables are the rest-mass density ρ and the specific internal energy $\varepsilon = \epsilon/\rho - 1$. The thermodynamical description of the fluid is specified by supplying an appropriate equation of state $p = p(\epsilon, q)$, which also involves the charge density of the fluid, describing the contribution of the Coulomb interaction between the fluid particles to the total pressure.

We build our model by considering a non-conductive ($\sigma = 0$) charged test fluid (taken to be a perfect fluid) in an axially symmetric spacetime and use spherical polar coordinates (t, r, θ, ϕ). The fluid rotates in the ϕ-direction with 4-velocity $U^\alpha = (U^t, U^\phi, 0, 0)$, specific angular momentum $\ell = -U_\phi/U_t$ and angular velocity (related to distant observers) $\Omega = U^\phi/U^t$, related by the formulae

$$\Omega = -\frac{\ell g_{tt} + g_{t\phi}}{\ell g_{t\phi} + g_{\phi\phi}}, \tag{9}$$

$$(U_t)^2 = \frac{g_{t\phi}^2 - g_{tt} g_{\phi\phi}}{\ell^2 g_{tt} + 2\ell g_{t\phi} + g_{\phi\phi}} \tag{10}$$

By writing out the covariant derivative of the electromagnetic part of the stress-energy tensor (8) appearing the left hand side of the conservation law (1), moving it to the right hand side, and using the Maxwell equations (2), with

$$\nabla_\beta F^{\alpha\beta}_{\rm EXT} = 0, \quad \nabla_\beta F^{\alpha\beta}_{\rm INT} = 4\pi J^\alpha, \tag{11}$$

we obtain the equation $\nabla_\beta T^{\alpha\beta}_{\rm MAT} = F^{\alpha\beta} J_\beta$, with J_β being the 4-current density due to the motion of the charged fluid torus. We are not here including the effects of the electromagnetic field generated by this 4-current: our tori are considered as being composed of 'test matter' from the electromagnetic point of view as well as from the gravitational one, i.e., $F^{\alpha\beta}_{\rm INT} \ll F^{\alpha\beta}_{\rm EXT}$ and we can write $F^{\alpha\beta} = F^{\alpha\beta}_{\rm EXT}$. Then we get the master equation

$$\nabla_\beta T^{\alpha\beta}_{\rm MAT} = F^{\alpha\beta}_{\rm EXT} J_\beta. \tag{12}$$

Note that in this approach we do not need to solve Maxwell's equations (2), since the electromagnetic field is prescribed. Also, because of the non-conductivity, we have

$$J^\alpha = q U^\alpha. \tag{13}$$

The equations of motion (12) give two non-linear partial differential equations for the pressure p, whose profiles we are wanting to find:

$$\begin{aligned}
\partial_r p &= -(\epsilon + p)\left(\partial_r \ln(U_t) - \frac{\Omega \partial_r \ell}{1 - \Omega\ell}\right) - q\, F_{r\alpha} U^\alpha \equiv \mathcal{R}, \\
\partial_\theta p &= -(\epsilon + p)\left(\partial_\theta \ln(U_t) - \frac{\Omega \partial_\theta \ell}{1 - \Omega\ell}\right) - q\, F_{\theta\alpha} U^\alpha \equiv \mathcal{T},
\end{aligned} \tag{14}$$

where $\mathcal{R} = \mathcal{R}(r, \theta)$ and $\mathcal{T} = \mathcal{T}(r, \theta)$. These equations are not integrable unless the integrability condition

$$\partial_\theta \mathcal{R} = \partial_r \mathcal{T} \tag{15}$$

is satisfied, and this is therefore a requirement.

The existence of a solution is guaranteed if $q = 0$, so that the last terms in equations (14) vanish and we get the Euler equation describing a rotating uncharged perfect fluid (see, e.g., papers [2, 3]). In this case, when the angular momentum distribution $\ell = \ell(r, \theta)$ is chosen, a solution of the Euler equation for any barotropic fluid (having $p = p(\epsilon)$) can be derived from Boyer's condition [2, 3]

$$\int_0^p \frac{{\rm d}p}{p + \epsilon} = W_{\rm in} - W, \tag{16}$$

$$W_{\rm in} - W = \ln(U_t)_{\rm in} - \ln(U_t) + \int_{\ell_{\rm in}}^{\ell} \frac{\Omega {\rm d}\ell}{1 - \Omega\ell}, \tag{17}$$

where the subscript 'in' refers to the inner edge of the torus in the equatorial plane. This condition enables us to straightforwardly determine the isobaric surfaces in the torus in terms of the equipotential surfaces of the 'gravito-centrifugal' potential $W(r, \theta)$: for equilibrium toroidal configurations composed of barotropic perfect fluid, the equipotential surfaces of W correspond to surfaces of constant pressure (or energy density) in the fluid.

When $q \neq 0$, the situation is more complicated and equations (14) are no longer integrable for arbitrary $q(r, \theta) = $ const and arbitrarily chosen $\ell = \ell(r, \theta)$. It is then necessary either to specify $\ell = \ell(r, \theta)$ (with even $\ell = $ const being possible) and find an appropriate $q = q(r, \theta)$ which is consistent with that or, vice versa, to specify $q = q(r, \theta)$ (with even $q = $ const being possible) and find an appropriate $\ell = \ell(r, \theta)$. However, this is strictly 'necessary' only if the equation of state is prescribed. Otherwise, one could also absorb the constraint into that. The charged tori must clearly have distributions of charge and angular momentum which satisfy the integrability condition.

III. ISOBARIC SURFACES IN REISSNER-NORDSTRÖM GEOMETRY

The Reissner-Nordström metric, representing the space-time outside a charged, non-rotating black hole, provides a suitable mathematically-simple test example for experimenting with ideas before moving on to more complicated examples having direct astrophysical relevance. In the dimensionless ($M = 1$) Schwarzschild coordinates, the only free parameter in the line element of the Reissner-Nordström geometry

$$\begin{aligned}
{\rm d}s^2 = &-\left(1 - \frac{2}{r} + \frac{Q^2}{r^2}\right){\rm d}t^2 + \left(1 - \frac{2}{r} + \frac{Q^2}{r^2}\right)^{-1} {\rm d}r^2 \\
&+ r^2({\rm d}\theta^2 + \sin^2\theta {\rm d}\phi^2)
\end{aligned} \tag{18}$$

is the dimensionless charge Q, which takes values $|Q| \leq 1$ for black-hole spacetimes and $|Q| > 1$ for naked-singularity spacetimes. The locations of event horizons, corresponding to the pseudo-singularities of the geometry, are given by solutions of the equation $\Delta \equiv r^2 - 2r + Q^2 = 0$. The ambient electric field is static and spherically symmetric, like the space-time, and is

described by the vector potential $A_\alpha = (A_t, 0, 0, 0)$, with the non-zero component being given by

$$A_t = -\frac{Q}{r}. \tag{19}$$

In this background, the pressure equations (14) reduce to the form

$$\begin{aligned} \partial_r p &= -(p+\epsilon)\left(\partial_r \ln|U_t| - \frac{\Omega\partial_r\ell}{1-\Omega\ell}\right) + q\,U^t\partial_r A_t, \\ \partial_\theta p &= -(p+\epsilon)\left(\partial_\theta \ln|U_t| - \frac{\Omega\partial_\theta\ell}{1-\Omega\ell}\right), \end{aligned} \tag{20}$$

where

$$U_t = -\frac{r\sin\theta\sqrt{\Delta}}{\sqrt{r^4\sin^2\theta - \ell^2\Delta}}. \tag{21}$$

To proceed further, it is then necessary to choose an equation of state. For an uncharged perfect fluid, a suitable choice is to have a polytropic relation between the pressure and the rest-mass density

$$p = \kappa\rho^\Gamma, \tag{22}$$

with κ and Γ being a polytropic constant and index. This widely-used relation is a convenient simple form which embodies conservation of entropy (as appropriate for a perfect fluid). For our calculations, we have used $\kappa = 10^{12}$ and $\Gamma = 2$. This value of Γ is mathematically convenient for making analytic integrations and, while it is rather high for physical applications, the convenience makes its use consistent within the spirit of the present simple model. We have chosen a high value of κ, because electrostatic corrections to the equation of state then become negligible, so that we can continue to use this polytropic equation of state consistently even in the charged case (we comment further on this in section VI C). Moreover, we use values of ρ which are sufficiently low so that the medium is non-relativistic and the contribution of the internal energy to the total energy density is then negligible as well, i.e., $\epsilon \approx \rho$. This approximation is consistent also with the assumption of negligible self-electromagnetic-field.

In order to find a solution for the pressure p, it is useful to rewrite equations (20) as equivalent equations for the density

$$\begin{aligned} \partial_r\rho &= \frac{(\kappa\rho^\Gamma+\rho)\left(\partial_r \ln|U_t| - \frac{\Omega\partial_r\ell}{1-\Omega\ell}\right) - q\,U^t\partial_r A_t}{-\Gamma\kappa\rho^{\Gamma-1}}, \\ \partial_\theta\rho &= \frac{(\kappa\rho^\Gamma+\rho)\left(\partial_\theta \ln|U_t| - \frac{\Omega\partial_\theta\ell}{1-\Omega\ell}\right)}{-\Gamma\kappa\rho^{\Gamma-1}}, \end{aligned} \tag{23}$$

which can be solved more easily than the ones for the pressure. On the other hand, in the uncharged case, the pressure profiles are determined from relation (16) which, for a polytropic equation of state, gives the following relatively simple analytic formula

$$p = \left(\frac{\mathrm{e}^{\frac{\Gamma-1}{\Gamma}(W_{\rm in}-W)} - 1}{\kappa^{\frac{1}{\Gamma}}}\right)^{\frac{\Gamma}{\Gamma-1}}. \tag{24}$$

(Note that this formula is valid only in the region where $W_{\rm in} \geq W$).

In the next sections, we consider the commonly-used condition of constant specific angular momentum, $\ell =$ const [2–8, 8–10]. Tori with $\ell =$ const are particularly simple mathematically and are generally representative of those with a more general angular momentum profile, although some care needs to be taken when considering perturbations (these configurations are only marginally stable with respect to convective instability [42]).

IV. UNCHARGED TORI, $\ell =$ const

For a barotropic fluid, the isobaric surfaces coincide with the equipotential surfaces of the potential $W(r,\theta)$, which are given by the formula

$$W(r,\theta) = \ln|U_t| = \ln\frac{r\sqrt{\Delta}\sin\theta}{\sqrt{r^4\sin^2\theta - \ell^2\Delta}}. \tag{25}$$

One of the reality conditions here, $\Delta \geq 0$, restricts the existence of equipotential surfaces to the stationary region of the spacetime. The other one, $r^4\sin^2\theta - \ell^2\Delta > 0$, evaluated in the equatorial plane ($\theta = \pi/2$), corresponds to the restriction that non-massless particles must move more slowly than photons

$$\ell^2 < \ell^2_{\rm ph}(r;Q^2) \equiv \frac{r^4}{\Delta}, \tag{26}$$

where the function $\ell^2_{\rm ph}(r;Q^2)$ plays the role of the effective potential governing photon geodesic motion in the equatorial plane (see [43] where the more general case with a non-zero cosmological constant is discussed). For the purpose of classification, we only need to consider positive values of $\ell_{\rm ph}(r;Q^2)$, i.e., we define $\ell_{\rm ph}(r;Q^2) \equiv \frac{r^2}{\sqrt{\Delta}}$. The function $\ell_{\rm ph}(r;Q^2)$ has one local extremum (a minimum) outside of the outer black-hole horizon, $\ell_{\rm ph,c}(Q^2)$, located at $r_{\rm ph,c} = \frac{1}{2}(3+\sqrt{9-8Q^2})$, corresponding to the circular photon orbit in the equatorial plane.

The character of the equipotential surfaces is well represented by the behavior of the potential $W(r,\theta)$ in the equatorial plane, i.e., by the function $W_{\pi/2}(r) \equiv W(r,\theta=\pi/2)$. Since the orbits with vanishing gradient of W, i.e. those satisfying the conditions $\partial_r W(r,\theta) = \partial_\theta W(r,\theta) = 0$, correspond to loci with zero pressure gradients, the fluid has to follow geodesic motion there. The local extrema of W are located only in the equatorial plane. Evaluating the necessary condition $\partial_r W_{\pi/2}(r) =$

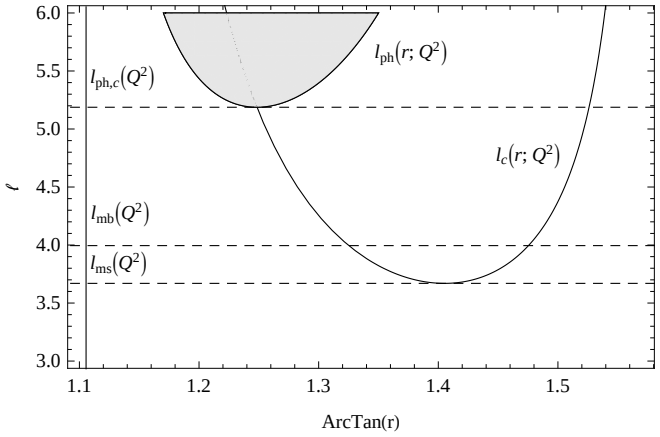

FIG. 1: Behavior of the function $\ell_{\rm c}(r;Q^2)$ governing extrema of the potential $W(r,\theta)$ in the equatorial plane of the Reissner-Nordström spacetime with $Q = 0.1$. For a fixed value of the angular momentum ℓ, we can determine the position of the potential maxima (smaller radius) and minima (larger radius). The potential $W(r,\theta)$ is not defined in the shaded region limited by the function $\ell_{\rm ph}(r;Q^2)$. In black-hole spacetimes ($Q^2 \leq 1$), there is only the class of the mutual behavior of the functions $\ell_{\rm c}(r;Q^2)$ and $\ell_{\rm ph}(r;Q^2)$, shown in this figure. The horizontal dashed lines denote the values of $\ell_{\rm ms}(Q^2) \doteq 3.670$, $\ell_{\rm mb}(Q^2) \doteq 3.995$ and $\ell_{\rm ph,c}(Q^2) \doteq 5.187$ for $Q = 0.1$, the value of Q being considered here, and the vertical solid line shows the position of the outer black-hole horizon. From the discussion of the behavior of $W(r,\theta)$ (see Fig. 2), it follows that equilibrium toroidal configurations of a barotropic fluid with $\ell = {\rm const}$ exist only for $\ell > \ell_{\rm ms}(Q^2)$.

0, these extrema are given by the condition

$$\ell^2 = \ell_{\rm c}^2(r;Q^2) \equiv \frac{r^4(r-Q^2)}{\Delta^2}. \qquad (27)$$

Again, for the purpose of classification, we only need to consider positive values of $\ell_{\rm c}(r;Q^2)$. This function has one local minimum $\ell_{\rm ms}(Q^2)$ corresponding to the specific angular momentum of the marginally stable orbit. In addition to the limiting values $\ell_{\rm ph,c}(Q^2)$ and $\ell_{\rm ms}(Q^2)$, there is also another one, $\ell_{\rm mb}(Q^2)$, corresponding to the specific angular momentum of a particle moving along the marginally bound equatorial circular geodesic, determined by the conditions $\partial_r W_{\pi/2}(r) = 0$ and $W_{\pi/2}(r) = 0$.

Independently of the charge parameter $|Q| \leq 1$ (we do not consider naked singularity spacetimes here), there is only one type of mutual behavior for $\ell_{\rm ph}(r;Q^2)$ and $\ell_{\rm c}(r;Q^2)$. We show this in Fig. 1, drawn for $Q = 0.1$ which we take as a standard value in the following. (Note that while this value for Q is rather high from an astrophysical point of view [44], it still gives only very small deviations of the space-time away from that of the Schwarzschild metric; taking a value this high is useful for clearly demonstrating the effects which we are wanting to investigate.)

Equilibrium toroidal configurations of a barotropic fluid with constant specific angular momentum exist only for $\ell > \ell_{\rm ms}(Q^2)$, which takes values ranging from $l_{\rm ms}(0) = 3.674$, corresponding to the Schwarschild limit, to $l_{\rm ms}(1) = 3.079$, corresponding to the extreme Reissner-Nordström black hole limit. Moreover, an important feature of constant specific angular momentum tori is that those which can form a cusp are limited by $l < l_{\rm mb}(Q^2)$, which takes values ranging from $l_{\rm mb}(0) = 4$ to $l_{\rm mb}(1) = 3.330$. The limit $l_{\rm mb}(0) = 4$ for the Schwarzschild case was also found for self-gravitating tori [26]. The radii given by the condition $\ell = \ell_{\rm c}(r;Q^2)$ then correspond to motion of fluid elements along the unstable circular geodesic (smaller radius) and the stable one (larger radius). The stable circular geodesic represents the 'center' of the torus (the potential $W(r,\theta)$ has a local minimum there while the pressure is maximal there). The unstable circular geodesic marks a critical point (cusp), where the potential $W(r,\theta)$ has a local maximum; the corresponding equipotential surface is self-crossing and is referred to as the 'critical surface'. As well as this critical equipotential surface, there is also the characteristic null equipotential surface $W(r,\theta) = 0$, which crosses the equatorial plane at infinity.

The behavior of the potential $W(r,\theta)$ can be summarized in the following way:

For $\ell \in (0, \ell_{\rm ms})$, there are no extrema of the potential W, and there are no closed equipotential surfaces and no critical equipotential surface. The null equipotential surface is open towards the black hole (Fig. 2A).

For $\ell = \ell_{\rm ms}$, there is one inflexion point of the potential W in the equatorial plane at which the critical surface has its critical point, corresponding to a ring. The null equipotential surface is open towards the black hole (Fig. 2B).

For $\ell \in (\ell_{\rm ms}, \ell_{\rm mb})$, there is a negative local maximum and a negative local minimum of the potential W in the equatorial plane. In this case, closed equipotential surfaces exist which are bounded by the critical surface that self-crosses at the inner cusp. The null equipotential surfaces is open towards the black hole (Fig. 2C).

For $\ell = \ell_{\rm mb}$, there is a zero local maximum and a negative local minimum of the potential W in the equatorial plane. The closed equipotential surfaces are bounded by the critical surface which coincides with the null equipotential surface (Fig. 2D).

For $\ell \in (\ell_{\rm mb}, \ell_{\rm ph,c})$, there is a positive local maximum and a negative local minimum of the potential W in the equatorial plane. The closed equipotential surfaces are bounded by the outer null equipotential surface. The critical surface is now open outwards away from the black hole, and self-crosses between the radii where the null surfaces cross the equatorial plane (Fig. 2E).

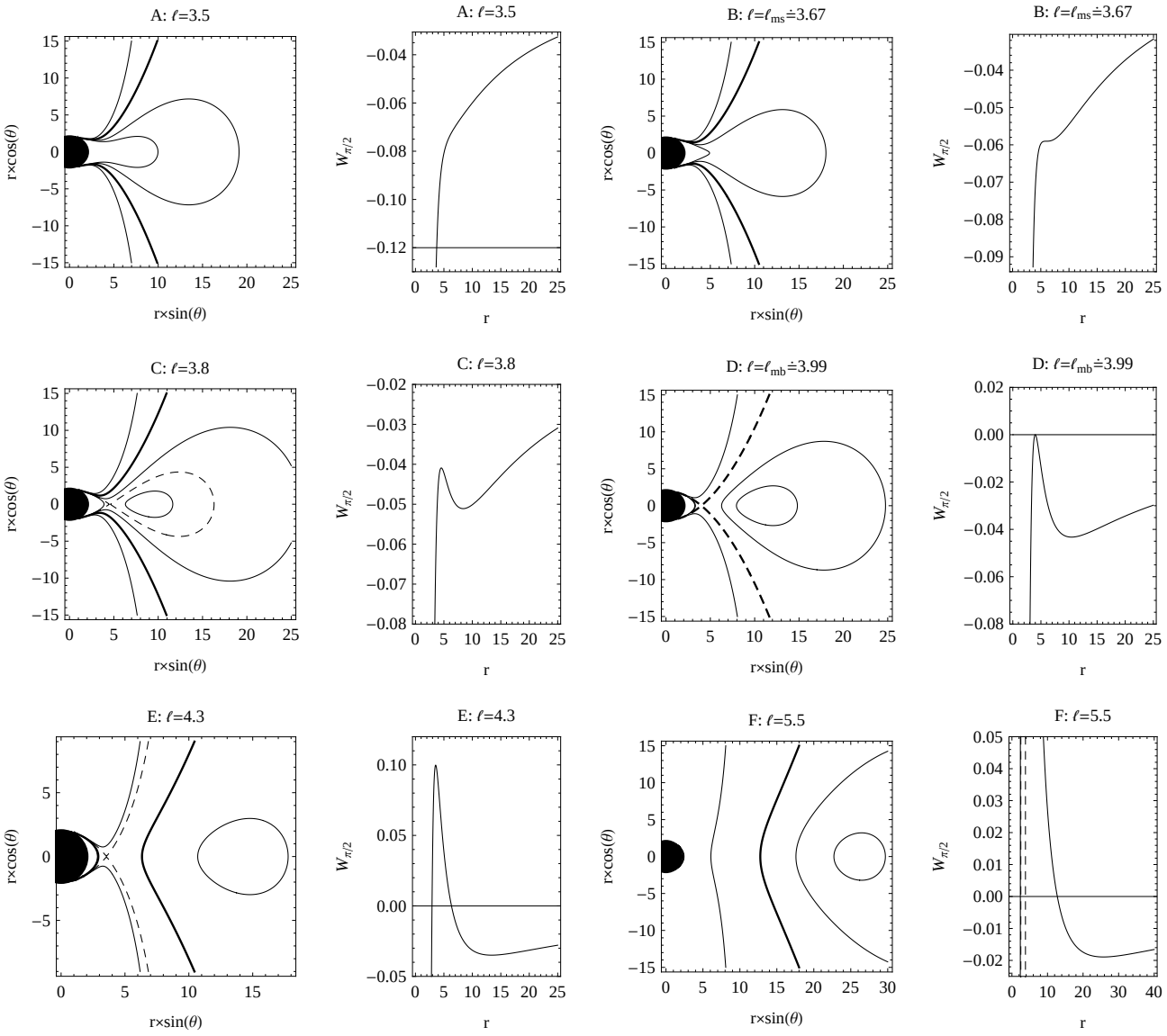

FIG. 2: Typical behavior of the potential $W(r,\theta)$ shown in terms of poloidal sections through the equipotential surfaces and the equatorial profile $W_{\pi/2}(r)$ in a Reissner-Nordström spacetime with parameter $Q = 0.1$. Taking progressively increasing values of the specific angular momentum ℓ, samples are shown of 4+2 qualitatively different types of behavior of the potential, differing in the properties of the critical (dashed) equipotential surface and the null (thick) equipotential surface.

For $\ell = \ell_{\rm ph,c}$, the potential W diverges at $r_{\rm ph,c}$ and the local maximum no longer exists. The negative local minimum of the potential W is still present. The closed equipotential surfaces are bounded by the outer null equipotential surface. The critical surface is no longer present.

For $\ell > \ell_{\rm ph,c}$, the only extremum of the potential W is the negative minimum. The closed equipotential surfaces are bounded by the outer null equipotential surface. There is no longer any critical surface, but there is a forbidden region for fluid elements with prescribed specific angular momentum, delimited by the radii satisfying the relation $\ell = \ell_{\rm ph}(r;Q^2)$ (Fig. 2F).

The behavior of the potential $W(r,\theta)$ is qualitatively the same as in the pure Schwarzschild case [3]. The additional charge of the black hole Q here influences the values of $\ell_{\rm ms}(Q^2)$, $\ell_{\rm mb}(Q^2)$ and $\ell_{\rm ph,c}(Q^2)$.

Profiles of the pressure and mass-density can now be determined from relations (24) and (22). For doing this, it is necessary to choose relevant values for the parameters of the polytropic equation of state (22), for the specific angular momentum and for the location of the inner edge of the torus. Here we present two examples, for tori with $\Gamma = 2$, $\kappa = 10^{12}$ and $\ell = 3.8$ (Fig. 3):

The first is the marginally bounded torus (the most extended closed torus), with its inner edge being at the

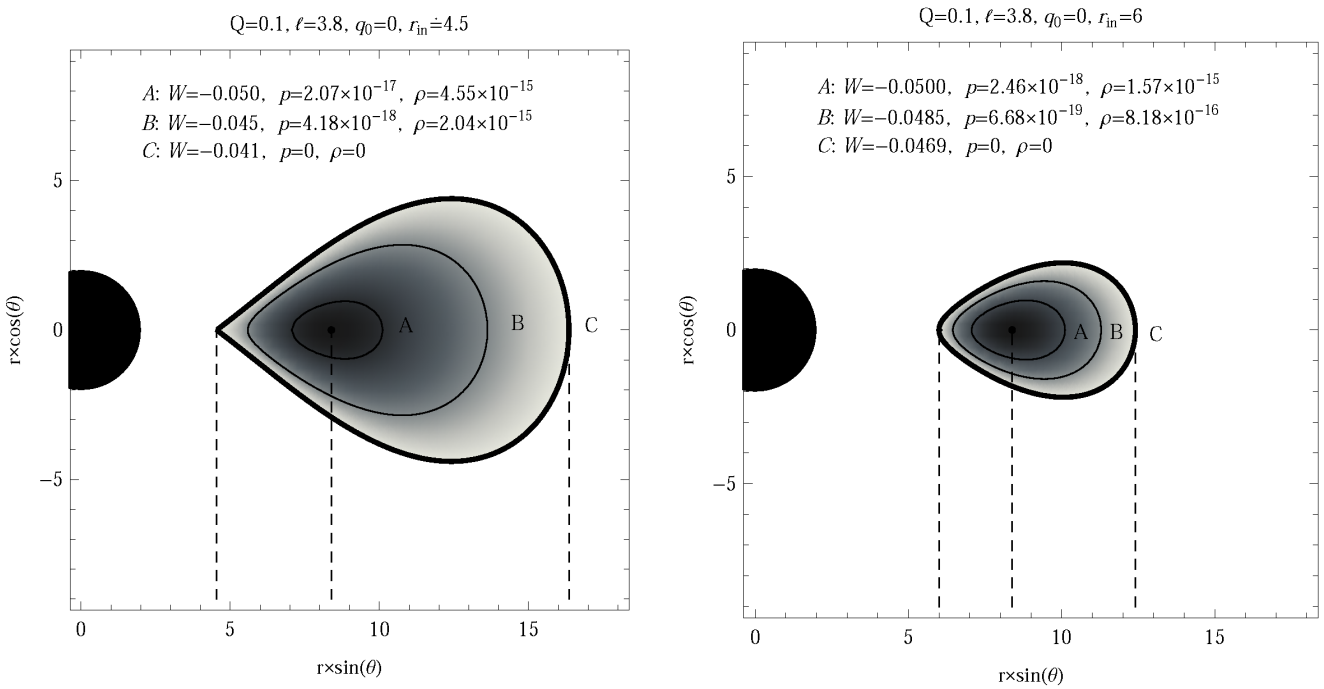

FIG. 3: Profiles of the potential $W(r,\theta)$, pressure $p(r,\theta)$ and rest-mass density $\rho(r,\theta)$ of uncharged tori, shown in terms of poloidal sections through the equipotential, isobaric and iso-density surfaces, respectively, and their equatorial behavior $W_{\pi/2}(r)$, $p_{\pi/2}(r)$ and $\rho_{\pi/2}(r)$, for a Reissner-Nordström spacetime with $Q = 0.1$. Two examples are shown with different values for the radius at the inner edge of the torus: $r_{\rm in} = r_{\rm cusp} \doteq 4.544$ in the upper figures and $r_{\rm in} = 6$ in the lower ones. The centers (pressure maxima) of both tori are located at $r_{\rm cent} \doteq 8.388$. The shapes of the equipotential, isobaric and iso-density surfaces coincide, with the values of the different quantities on them being related by equation (24) and the equation of state (22). We show poloidal sections through three such surfaces (A, B and C). The thick curve (surface C) marks the zero-pressure (and zero-density) surface which bounds the torus. The shaded regions above the profiles of $W_{\pi/2}(r)$ indicate the physically relevant parts of the profiles, delimited by the inner and outer edges of the tori. The specific angular momentum $\ell = 3.8$ for both tori, and the polytropic parameters are $\Gamma = 2$ and $\kappa = 10^{12}$ in each case.

cusp, $r_{\rm in} = r_{\rm cusp}$. This is the most interesting case, since it can be used as a model for the inner parts of a thick accretion disk from which matter can flow in a standard way onto the black hole. To obtain the position of the cusp, we solve equation (27), which yields two real roots above the event horizon; $r_{\rm I} \doteq 4.544$ and $r_{\rm II} \doteq 8.388$. The first root corresponds to the position of the unstable circular geodesic, i.e. to the cusp, while the second one corresponds to the stable geodesic, i.e to the pressure maximum: the 'center' of the torus.

Our second example is a torus with its inner edge located at $r_{\rm in} > r_{\rm cusp}$. Here we simply chose the position of the inner edge to be at $r_{\rm in} = 6$. Note that the location of the inner edge must be chosen so as to be in between the cusp ($r_{\rm I}$) and the center of the torus ($r_{\rm II}$), the positions of both of which are determined from the potential W independently of the choice of $r_{\rm in}$.

V. CHARGED TORI, $\ell = {\rm const}$

In order to obtain the pressure or density profiles from equations (20) or (23), it is necessary to determine the charge density distribution $q(r,\theta)$ in the torus. This must satisfy the integrability condition (15). By expressing $q(r,\theta)$ in the form

$$q(r,\theta) = q_0 \rho(r,\theta) k(r,\theta), \tag{28}$$

where q_0 is a constant and $k(r,\theta)$ is a correction function, and using $\Gamma = 2$, we can rewrite equation (23) in the form

$$\begin{aligned} \partial_r \rho &= -\frac{1}{2\kappa}\Big((\kappa\rho+1)\partial_r \ln|U_t| - q_0 k\, U^t \partial_r A_t\Big), \\ \partial_\theta \rho &= -\frac{1}{2\kappa}\Big((\kappa\rho+1)\partial_\theta \ln|U_t|\Big). \end{aligned} \tag{29}$$

Note that, as we express by relation (28), it is feasible to take the charge density distribution as being directly proportional to the rest-mass density distribution and to a correction function which represents variations in the charge per unit mass $q_0 k(r,\theta)$ through the torus, as we discuss in section VI A. From the mathematical point of view, the correction function plays the role of an 'integration factor', which must be chosen so that equations (29) are integrable.

Now, due to the integrability condition (15), the correction function $k(r,\theta)$ has to satisfy the relation

$$2\sin\theta(\ell^2\Delta - r^4\sin^2\theta)\partial_\theta k + 3k\ell^2\Delta\cos\theta = 0, \quad (30)$$

which can be solved to give

$$k(r,\theta) = \frac{\gamma}{\sin^{3/2}\theta}\left(\frac{\ell^2\Delta - r^4\sin^2\theta}{\ell^2\Delta - r^4}\right)^{3/4}, \quad (31)$$

where $\gamma(r)$ is a function representing a constant of integration over θ for a given value of k in the equatorial plane, $k(r,\theta=\pi/2)\equiv\gamma(r)$. For the purposes of this paper, it is convenient to choose $\gamma(r)=1$. The charge density distribution function with the correction function in the form (31) ensures the integrability of equations (29), and thus the existence of a unique solution for $p(r,\theta)$ and $\rho(r,\theta)$.

Integrating the second of equations (29) over the latitude, we obtain the following expression for the rest-mass density:

$$\rho(r,\theta) = \frac{2^{1/4}\kappa\, C\left(r^4\sin^2\theta - \ell^2\Delta\right)^{1/4} - \sqrt{\sin\theta}}{\kappa\sqrt{\sin\theta}}. \quad (32)$$

The unknown function $C(r)$, which depends only on the radial coordinate r, stands as a constant of this integration. Its value can be determined by substituting the density formula (32) into the first density equation (29) and assuming the charge-density distribution according to relations (28) and (31). This leads to the ordinary differential equation

$$2r\Delta\partial_r C + (2r^2 - 3r + Q^2)C = \frac{r^2\sqrt{\Delta}Qq_0}{2^{1/4}\kappa(r^4 - \ell^2\Delta)^{3/4}}. \quad (33)$$

Unfortunately, there is no analytic solution for equation (33), and so $C(r)$ must be determined numerically. Since the torus is delimited by the zero-pressure (and zero-density) surface, we can find the necessary initial condition from the fact that $\rho(r_{\rm in})=0$. From the relation (32) we obtain

$$C(r_{\rm in}) = \frac{1}{2^{1/4}\kappa[r_{\rm in}^4 - \ell^2(r_{\rm in}^2 - 2r_{\rm in} + Q^2)]^{1/4}}. \quad (34)$$

As mentioned earlier, the most interesting configuration is the one delimited by the self-crossing zero isobaric (and iso-density) surface, i.e., the marginally bounded torus, which has its inner edge in the equatorial plane coincident with the cusp ($r_{\rm in} = r_{\rm cusp}$). We will be concentrating on this type of torus from now on. The values of the specific angular momentum ℓ and the charges Q and q_0 then completely determine the shape of the torus and the positions of its center and of its inner and outer edges. At the cusp, the pressure and density vanish and have a saddle point (a minimum in the r-direction and a maximum in the θ-direction), in contrast with the center of the torus, where there is a local maximum. (In general, the density at the inner edge of the torus must be zero and when the inner edge is also a cusp, the density profile has extrema there.) The location of the inner edge $r_{\rm in}$, which needs to be known in order to evaluate the condition (34), can then be obtained from the first of equations (29) by setting $\partial_r\rho\big|_{r=r_{\rm in}} = 0$, $\rho(r_{\rm in})=0$, and $\theta=\pi/2$. This gives the following implicit expression for $r_{\rm in}$:

$$q_0 Q r_{\rm in}^2\sqrt{\Delta(r_{\rm in}^4 - \ell^2\Delta)} + (Q^2 - r_{\rm in})r_{\rm in}^4 + \ell^2\Delta^2 = 0. \quad (35)$$

Note that when $q_0=0$, we get the relation $(Q^2 - r_{\rm in})r_{\rm in}^4 + \ell^2\Delta^2 = 0$, in agreement with the formula (27) derived for the case of the uncharged torus.

To clearly illustrate how the charge on the torus affects its equilibrium structure, we constructed marginally-bounded tori with the same matter parameters and specific angular momentum as in the uncharged case, i.e., we took $\kappa = 10^{12}$ and $\ell = 3.8$, and we also considered the same charge of the central black hole $Q=0.1$. Our sample tori are characterized by the parameters $q_0 = 0.4$ (positively charged) and $q_0 = -0.4$ (negatively charged), which, as we discuss in section VI A, correspond to the specific charges of the moving matter in the equatorial plane, due to our choice $\gamma(r)=1$.

For $q_0 = 0.4$, equation (35) yields two real roots above the event horizon; $r_{\rm I} \doteq 4.378$ and $r_{\rm II} \doteq 9.104$, where both of the roots correspond to circular orbits of charged test particles with the given specific charge 0.4. Choosing $r_{\rm in} = r_{\rm I}$, the numerical integration gives a regular thick charged torus. On the other hand, choosing $r_{\rm in} = r_{\rm II}$, we get a degenerate torus (an infinitesimally thin ring) located just at $r = r_{\rm II}$.

For $q_0 = -0.4$, equation (35) again yields two real roots above the event horizon; $r_{\rm I} \doteq 4.767$ and $r_{\rm II} \doteq 7.658$, corresponding to circular orbits of charged test particles with the given specific charge -0.4. Again, the choice $r_{\rm in} = r_{\rm I}$ leads to the regular thick charged torus, while $r_{\rm in} = r_{\rm II}$ gives the degenerate torus.

In principle, one could also construct charged tori with $r_{\rm I} < r_{\rm in} < r_{\rm II}$, as for the uncharged tori. However, this introduces further complications, and we focus here only on the more interesting critical (cusp) configurations.

In Figs 4 and 6, we show the profiles of rest-mass density and pressure. The related charge density distributions $q(r,\theta)$ and correction functions $k(r,\theta)$ are shown in Figs 5 and 7. As can be seen from these, for the same Q and ℓ, the positively charged tori are more extended than the uncharged ones while the negatively charged tori are less extended. From the right-hand panels of Figs 4 and 6, it can be seen that the densities in the more extended tori are larger than those in the less extended ones and so the masses of the more extended tori are clearly also larger. We come back to this in more detail in section VI B.

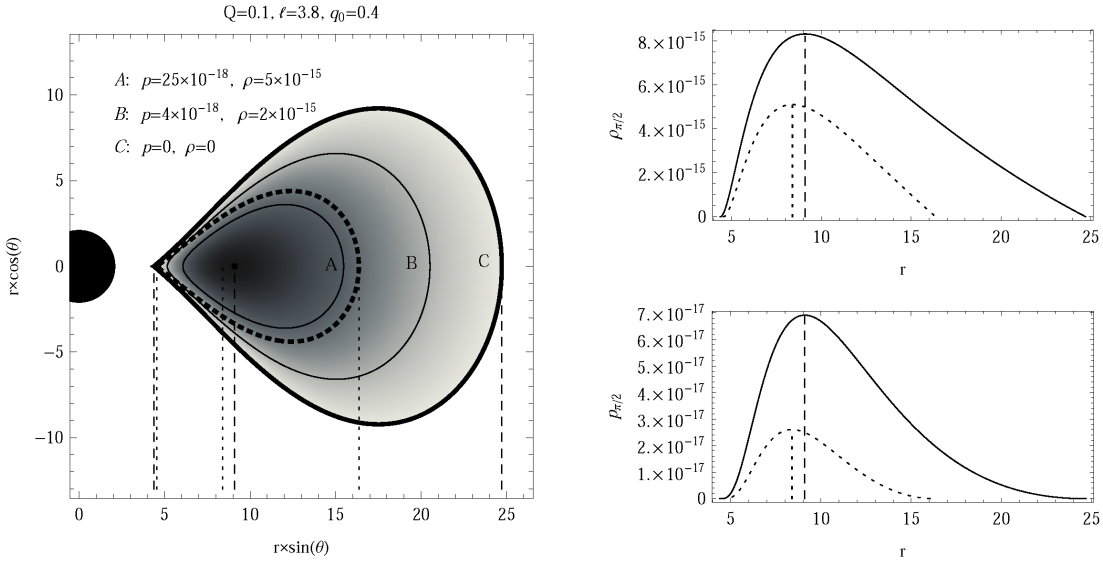

FIG. 4: Profiles of the pressure $p(r,\theta)$ and rest-mass density $\rho(r,\theta)$ for a positively charged torus ($q_0 = 0.4$, $\ell = 3.8$) in a Reissner-Nordström spacetime with $Q = 0.1$, shown in terms of poloidal sections through the isobaric and iso-density surfaces (left), and in terms of their equatorial profiles $p_{\pi/2}(r)$ and $\rho_{\pi/2}(r)$ (right). The torus terminates at $r_{\rm in} = r_{\rm cusp} \doteq 4.378$ and $r_{\rm out} \doteq 24.72$, and its center is located at $r_{\rm cent} \doteq 9.098$. The dashed curves represent the zero-pressure surface for the equivalent uncharged case (left panel) and the profiles of density and pressure for the uncharged case (right panels). The isobaric and iso-density surfaces coincide (A, B and C), with the values of pressure and density on them being related by the equation of state.

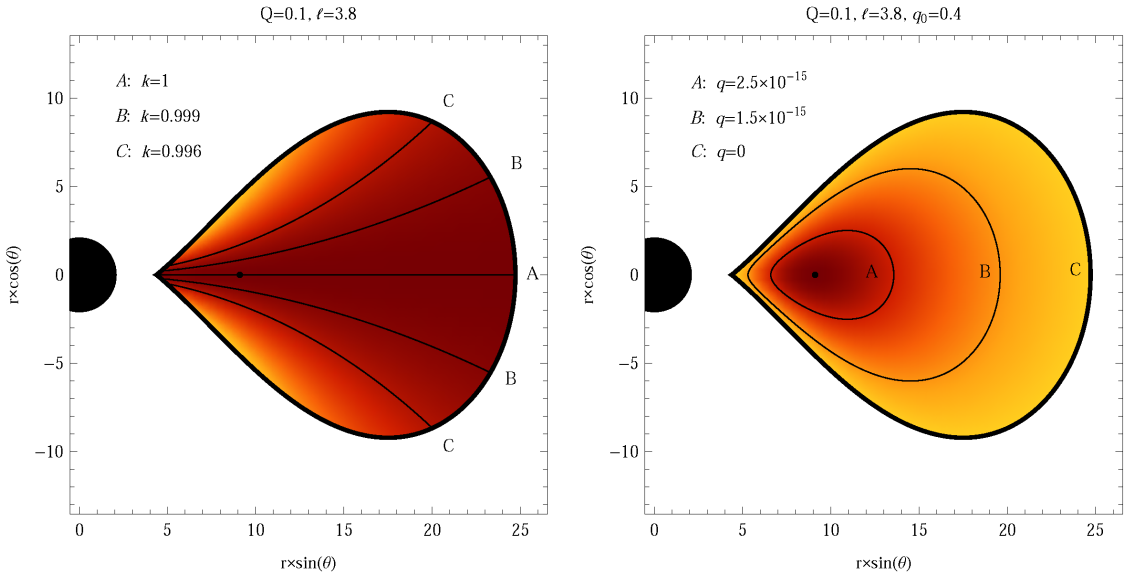

FIG. 5: Poloidal sections through the iso-contours for the correction function $k(r,\theta)$ (left) and the charge density $q(r,\theta)$ (right) for the same positively charged torus as in Fig. 4.

VI. DISCUSSION

A. Correction function and specific charge

The dimensionless correction function $k(r,\theta)$ has been introduced in equation (28) for convenience in calculating the torus configuration. It represents the variation with position of the specific electric charge (charge per unit mass), $\bar{q} = q_0 k(r,\theta)$. As shown in the previous section, setting $k = 1$ so that the charge per unit mass is the same everywhere, does not give an equilibrium configuration: k must be allowed to vary so as to satisfy the integrability

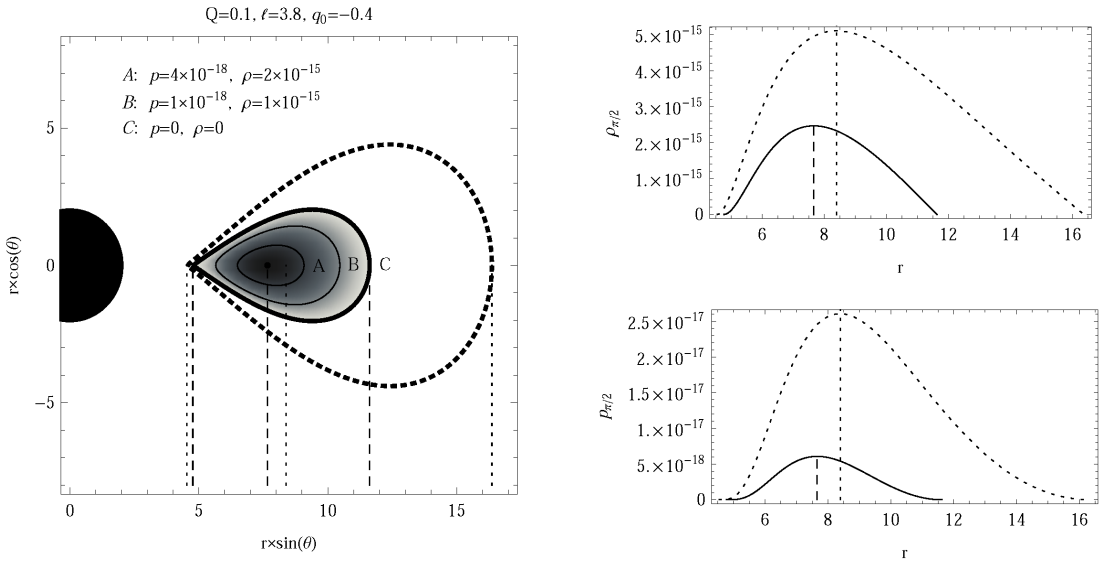

FIG. 6: Profiles of the pressure $p(r,\theta)$ and rest-mass density $\rho(r,\theta)$ for a negatively charged torus ($q_0 = -0.4$, $\ell = 3.8$) in a Reissner-Nordström spacetime with $Q = 0.1$, shown in terms of poloidal sections through the isobaric and iso-density surfaces (left), and in terms of their equatorial profiles $p_{\pi/2}(r)$ and $\rho_{\pi/2}(r)$ (right). The torus terminates at $r_{\rm in} = r_{\rm cusp} \doteq 4.767$ and $r_{\rm out} \doteq 11.62$, and its center is located at $r_{\rm cent} \doteq 7.660$. The dashed curves represent the zero-pressure surface for the equivalent uncharged case (left panel) and the profiles of density and pressure for the uncharged case (right panels). The isobaric and iso-density surfaces coincide (A, B and C), with the values of pressure and density on them being related by the equation of state.

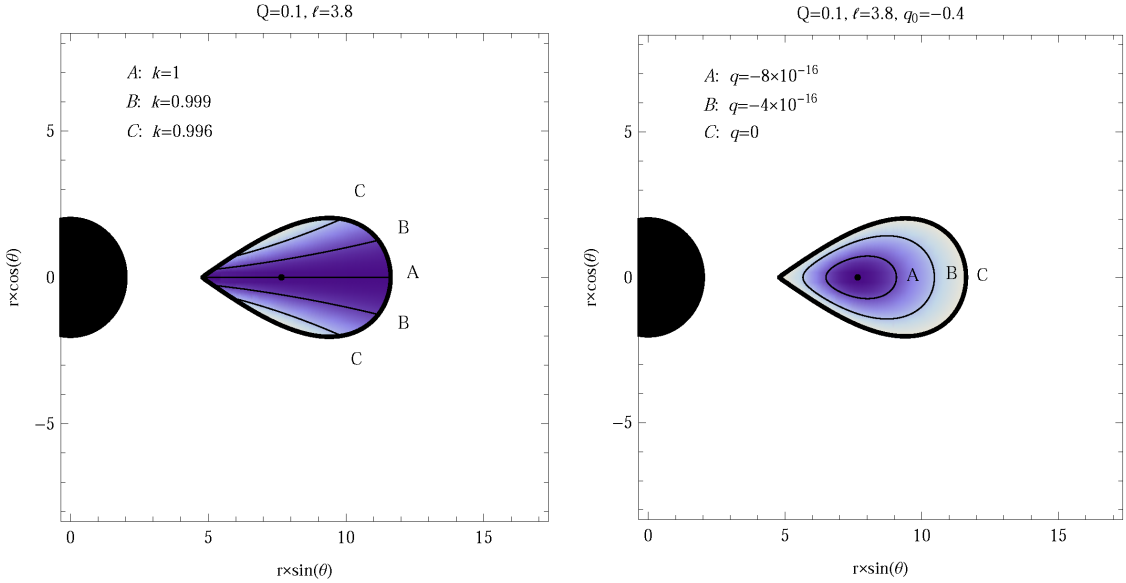

FIG. 7: Poloidal sections through the iso-contours for the correction function $k(r,\theta)$ (left) and the charge density $q(r,\theta)$ (right) for the same negatively charged torus as in Fig. 6.

condition (15) and this requires the behavior (31). In the equatorial plane $k(r,\theta = \pi/2) = \gamma(r)$, and the choice $\gamma(r) = 1$ as a boundary condition is convenient for our present simplified model. From Figs (5) and (7), it can be seen that the required variations in $k(r,\theta)$ away from this are actually very small (with the maximum being on the equatorial plane).

Our choice of $\gamma(r) = $ const (with the constant normalised to 1) corresponds to a case where the maximum of the charge density $q(r,\theta)$ is located just at the center of the torus, where there is the maximum of the density $\rho(r,\theta)$, as can be seen from relation (28). Other choices of

$\gamma(r)$ could describe more physically relevant situations, but with the maximum of $q(r,\theta)$ not necessarily being located at the center of the torus. For instance, by choosing $\gamma(r) = 1/r$ the specific net charge of the fluid in the torus grows in the equatorial plane from the outer edge to the inner edge, where it is maximal. Moreover, the maximum of $q(r,\theta)$ is shifted from the center of the torus. Of course, at the inner edge, the net charge density $q(r,\theta)$ goes to zero together with the matter density $\rho(r,\theta)$.

The values $q_0 = \pm 0.4$ and $\gamma = 1$, used for our representative cases, give a specific charge $\bar{q}$ in the torus around 10^{18} times smaller in magnitude than that for a proton, and so the medium can be thought of as having one particle in 10^{18} with a net charge while the rest are neutral. We note that if we decrease Q below our standard value of 0.1 and simultaneously increase q_0 in such a way that the product $Q\bar{q}$ remains unchanged, then we get essentially identical results. This is because the deviation of the space-time geometry away from Schwarzschild is extremely small for these values of Q, and so the relevant effect of the charge is almost entirely electromagnetic (depending on $Q\bar{q}$) rather than having a significant gravitational contribution (depending just on Q).

B. Total electric charge and mass of the torus

In our model, we neglect the effects of the electromagnetic field generated by the torus, which is acceptable when this self-field is much weaker than the external electromagnetic field associated with the central compact object. The total charge of the torus is given by

$$\begin{aligned} \mathcal{Q} &= \int_V q\sqrt{-g}\,\mathrm{d}r\,\mathrm{d}\theta\,\mathrm{d}\phi \\ &= 4\pi q_0 \int_{r_{\rm in}}^{r_{\rm out}} \int_{\theta_{\rho_0}}^{\frac{\pi}{2}} k\rho\sqrt{-g}\,\mathrm{d}\theta\,\mathrm{d}r, \end{aligned} \tag{36}$$

where

$$\theta_{\rho_0} = \arcsin\left(\frac{\sqrt{2\Delta}\kappa^2\ell C^2}{\sqrt{2\kappa^4 r^4 C^4 - 1}}\right) \tag{37}$$

is the function determining the upper boundary of the poloidal projection of the zero isodensity surface, $g = -r^4\sin^2\theta$ is the determinant of the metric tensor, and $r_{\rm out}$ is the radial position of the outer edge of the torus in the equatorial plane. For the representative tori which we are considering, with $\Gamma = 2$, $\kappa = 10^{12}$, $Q = 0.1$ and $\ell = 3.8$, we obtain the total charge on the torus as being $\mathcal{Q} \doteq 2.49 \times 10^{-11}$ for $q_0 = 0.4$ (positively charged) and $\mathcal{Q} \doteq -4.50 \times 10^{-13}$ for $q_0 = -0.4$ (negatively charged). Such small values, in comparison with the charge of the black hole, are consistent with our neglect of the electromagnetic field generated by the torus.

The total rest-mass of the torus is given by

$$\begin{aligned} \mathcal{M} &= \int_V \rho\sqrt{-g}\,\mathrm{d}r\,\mathrm{d}\theta\,\mathrm{d}\phi \\ &= 4\pi \int_{r_{\rm in}}^{r_{\rm out}} \int_{\theta_{\rho_0}}^{\frac{\pi}{2}} \rho\sqrt{-g}\,\mathrm{d}\theta\,\mathrm{d}r. \end{aligned} \tag{38}$$

For the three representative tori which we are considering, we obtain the total rest-mass as being $\mathcal{M} \doteq 6.24 \times 10^{-11}$ (positively charged), $\mathcal{M} \doteq 1.13 \times 10^{-12}$ (negatively charged) and $\mathcal{M} \doteq 9.64 \times 10^{-12}$ (uncharged). The ratio $\mathcal{Q}/\mathcal{M}$ is then $\doteq \pm 0.4$ in the positively and negatively charged cases, respectively, as clearly follows from the fact that the specific charge $\bar{q} = q_0 k(r,\theta) = \pm 0.4 k(r,\theta) \doteq \pm 0.4$, since $k(r,\theta) \approx 1$ throughout our tori.

C. Parameters of the equation of state

We set $\Gamma = 2$ for illustration purposes, since this choice simplifies the integration of the density equations (23). This value of Γ is inconveniently high for possible related astrophysical applications, but we stress that our model is an extremely simplified one, purposely intended for investigating the behavior of a test case under extreme conditions (we are also taking a rather large value for the black-hole charge Q, only one sign of charge for particles in the torus and zero conductivity there). For such a test case, it would not be appropriate to introduce additional complications here in order to bring just one aspect of the model (the value of Γ) closer to astrophysical applications.

In general, electrostatic corrections should also be included in the equation of state, especially at higher matter densities. However, this is not trivial to do (see, e.g. [45], for the electrostatic correction in the case of dusty plasmas). We have used a very high value of κ, which enables us to neglect electrostatic corrections without inconsistency, because this enables us to demonstrate our approach more clearly.

D. Distribution of specific angular momentum

We have considered perfect-fluid tori with a prescribed specific angular momentum $\ell = -U_\phi/U_t$, which we set to be constant through the torus. In an uncharged case, $L = U_\phi$ and $E = -U_t$ would be constants of motion connected with the assumed axial symmetry and stationarity of the spacetime. For a charged torus, the constants of motion are the generalized quantities $\tilde{L} = U_\phi + \bar{q}A_\phi$ and $\tilde{E} = -U_t - \bar{q}A_t$.

Note that the condition $\ell = \text{const}$ is imposed for simplicity of the calculations; it is not essential for the method and can be relaxed. The Rayleigh criterion for linear stability against radial convection requires ℓ to be a non-decreasing function of the distance from the axis of rotation, and so $\ell = \text{const}$ uncharged tori are just on

the stability limit. For charged tori, the stability condition needs to be formulated in terms of a generalized quantity $\tilde{\ell} = \tilde{L}/\tilde{E}$ [30, 46]. In the Reissner-Nordström electric field, the only non-zero component of the vector potential is A_t and one has

$$\tilde{\ell} = \frac{\tilde{L}}{\tilde{E}} = \frac{L}{E - q_0 k A_t}, \tag{39}$$

which reduces to ℓ for $q_0 = 0$. Stability depends heavily on the specific charge distribution (i.e. on the behavior of the correction function $k(r, \theta)$) and on the signs of the charges of the torus and the black hole.

E. Approximation of negligible conductivity

The assumption of high electrical conductivity of the medium is appropriate for many astrophysical plasmas with a high degree of ionization, and the ideal MHD framework can then be employed. Under the conditions of high conductivity and vanishing inertial effects of the plasma particles, the local electric field quickly becomes neutralized by rearranging the plasma flows (giving the conditions for the force-free approximation). A quasi-neutral medium then arises in which the volume density of net electric charge is negligible.

However, there is an ongoing debate about the conditions that may lead to the presence of non-vanishing net charges, with an important role being played by electric forces acting parallel to the magnetic field lines in the local co-moving frame. For example, a large-scale magnetic field may cause spatial separation of electric charges of different signs and their gradual accumulation in different parts of the system. Pulsar magnetospheres provide an example of such systems, with the charge separation being caused by the dipole-type magnetic field of the neutron star [47, 48]. Black holes embedded in ordered magnetic fields of external origin can also act in a similar way but then, for a low-density medium, the hydrodynamical description needs to be modified in order to describe the conditions of a collisionless plasma (since the particle mean-free paths are then comparable with the characteristic length-scale of the system, given by the gravitational radius of the central black hole).

One can imagine also another relevant scenario: a neutral fluid containing a few free charges, such as the case of dusty plasmas. In general, when charges feel an external electromagnetic field, they move generating a current, but if the fluid is dense enough and is highly collisional, the charges are less able to move and the conductivity becomes almost zero (see [49] for a discussion). Such a picture is actually compatible with our model since, as mentioned earlier, only a very small fraction of particles with net charge is required in order to give the parameter values used in our representative examples.

F. Zero conductivity and consistency of the model

The various limiting situations which we have been mentioning (hydrodynamical versus collisionless plasma; infinite conductivity versus zero conductivity; self-gravitating matter versus test particles and fluids), are relevant under quite different circumstances and obviously require different approaches. The approach which we have adopted in the present paper allows us to capture the behavior of an idealized but non-trivial system where the fluid motion is governed by the combined action of a global (large-scale) electromagnetic field, the gravitational field of the central body, and pressure gradients operating within the fluid together with a non-zero electric charge distribution.

The basic assumptions of our model are: 1) the fluid is a single-component test fluid (we ignore its self-gravity and its own electromagnetic field); 2) the fluid flow is stationary, with the 4-velocity having only time and azimuthal components. If the conductivity σ were non-zero, the second term on the right-hand side of the Ohm's law equation (4), which is proportional to σ, would give rise to a radial electric current unless there were a significant self-field (contradicting the first basic assumption). Since our fluid is taken to be a single-species one, having a radial electric current would imply the existence of a radial mass current (contradicting the second basic assumption). Having $\sigma = 0$ is therefore necessary for self-consistency.

VII. CONCLUSIONS

In this paper we have presented a model for a simple test case of an electrically-charged perfect-fluid torus rotating in strong gravitational and electromagnetic fields produced by a central compact object. Distributions of either specific angular momentum or charge density through the torus first need to be specified (we chose to specify the specific angular momentum distribution) and then pressure and density profiles can be calculated. An equation of state must be provided in order to close the set of equations. We have investigated the limiting case opposite to that of ideal magnetohydrodynamics, considering a non-conductive (dielectric) perfect fluid rather than infinite conductivity as in ideal magnetohydrodynamics. Our case can describe a fluid in which bulk hydrodynamic motion predominates over electromagnetic effects and the fluid has almost infinite electric resistivity. We are not here including the self-gravitational and self-electromagnetic fields of the matter in the torus, and so the treatment applies for low-mass, slightly-charged tori.

For illustrating the model, we constructed both positively and negatively charged barotropic tori, with a polytropic equation of state and constant specific angular momentum distribution, encircling a positively-charged Reissner-Nordström black hole. We compared the re-

sulting pressure and density profiles with an equivalent uncharged case, and also calculated the shapes of the tori. Taking the polytropic index $\Gamma = 2$, allows for the 'pressure' equation to be integrated in a relatively simple way so as to give semi-analytic results. The large value for the polytropic constant $\kappa = 10^{12}$ leads to tori where the Coulomb interaction between the charged particles of the fluid can be neglected in comparison with the standard pressure due to the matter. The constructed tori are only slightly electrically charged in comparison with the charge of the black hole, thus generating a relatively weak electromagnetic field which can safely be neglected. It is striking that even with a very small value for the charge-to-mass ratio in the torus, significant effects are nevertheless seen. However, it is necessary to stress out that the constructed tori carry the specific charge $\mathcal{Q}/\mathcal{M} \doteq \pm 0.4$ and orbit the black hole with $Q/M = 0.1$; since for any astrophysical body it would be practically impossible to maintain the specific charge $Q/M > 10^{-18}$ [44], the results should be considered as illustrating samples only.

The aim of this paper has been to introduce a new model of a dielectric charged torus encircling a charged compact object. We have proceeded by using a number of simplifying assumptions: the compact object is a Reissner-Nordström black-hole; the torus is composed of test matter; the matter has a polytropic equation of state with prescribed Γ; the torus has constant specific angular momentum, $\ell = \text{const}$, and the specific charge is constant everywhere in the equatorial plane, $\gamma = 1$. Despite the great simplifications coming from these assumptions, the scenario is still physically reasonable and non-trivial. Moreover, a large variety of degrees of freedom can be captured and the free parameters can be conveniently chosen in order to describe an astrophysically relevant situation. Of course, more complicated choices would then require more complicated calculations. Such calculations are now in progress, but are beyond the scope of the present paper.

Acknowledgments

The Opava Institute of Physics and Prague Astronomical Institute have been operated under the projects MSM 4781305903 and AV 0Z10030501, and further supported by the Center for Theoretical Astrophysics LC06014 in the Czech Republic. JK, VK and ZS thank the Czech Science Foundation (ref. P209/10/P190, 205/07/0052, 202/09/0772). We also gratefully acknowledge support from CompStar, a Research Networking Programme of the European Science Foundation and thank an anonymous referee for advice and critical comments which have led to improvement of our paper.

[1] J. Frank, A. King, and D. Raine, *Accretion Power in Astrophysics* (Cambridge University Press, 2002).
[2] M. Kozłowski, M. Jaroszyński, and M. A. Abramowicz, Astronomy and Astrophysics **63**, 209 (1978).
[3] M. A. Abramowicz, M. Jaroszyński, and M. Sikora, Astronomy and Astrophysics **63**, 221 (1978).
[4] Z. Stuchlík, P. Slaný, and S. Hledík, Astronomy and Astrophysics **363**, 425 (2000).
[5] J. A. Font and F. Daigne, Monthly Notices of the Royal Astronomical Society **334**, 383 (2002).
[6] L. Rezzolla, O. Zanotti, and J. A. Font, Astronomy and Astrophysics **412**, 603 (2003).
[7] Z. Stuchlík, Modern Phys. Lett. A **20**, 561 (2005).
[8] P. Slaný and Z. Stuchlík, Classical Quantum Gravity **22**, 3623 (2005).
[9] Z. Stuchlík, P. Slaný, and J. Kovář, Classical Quantum Gravity **26**, 215013 (2009).
[10] H. Kučáková, P. Slaný, and Z. Stuchlík, Journal of Cosmology and Astroparticle Physics **1**, 33 (2011).
[11] Z. Stuchlík and S. Hledík, Physical Review D **60**, 044006 (1999).
[12] B. Punsly, *Black hole gravitohydromagnetics* (Springer-Verlag Berlin Heidelberg, 2008).
[13] R. V. E. Lovelace, C. Mehanian, C. M. Mobarry, and M. E. Sulkanen, Astrophysical Journal Supplement Series **62**, 1 (1986).
[14] A. R. Prasanna, S. C. Tripathy, and A. C. Das, Journal of Astrophysics and Astronomy **10**, 21 (1989).
[15] S. C. Tripathy, A. R. Prasanna, and A. C. Das, Monthly Notices of the Royal Astronomical Society **246**, 384 (1990).
[16] P. Bhaskaran and A. R. Prasanna, Journal of Astrophysics and Astronomy **11**, 49 (1990).
[17] P. Bhaskaran, S. C. Tripathy, and A. R. Prasanna, Journal of Astrophysics and Astronomy **11**, 461 (1990).
[18] D. Banerjee, J. R. Bhatt, A. C. Das, and A. R. Prasanna, The Astrophysical Journal **449**, 789 (1995).
[19] D. Banerjee, J. R. Bhatt, A. Das, and A. R. Prasanna, The Astrophysical Journal **474**, 389 (1997).
[20] S. S. Komissarov, Monthly Notices of the Royal Astronomical Society **368**, 993 (2006).
[21] D. B. Melrose, *Plasma astrophysics. Nonthermal processes in diffuse magnetized plasmas* (New York: Gordon and Breach, 1980).
[22] S. Koide, The Astrophysical Journal **708**, 1459 (2010).
[23] C. Palenzuela, L. Lehner, O. Reula, and L. Rezzolla, Monthly Notices of the Royal Astronomical Society **394**, 1727 (2009).
[24] T. Kudoh and O. Kaburaki, The Astrophysical Journal **460**, 199 (1996).
[25] S. Nishida and Y. Eriguchi, The Astrophysical Journal **427**, 429 (1994).
[26] N. Stergioulas, International Journal of Modern Physics D **20**, 1251 (2011).
[27] V. Karas, J.-M. Huré, and O. Semerák, Classical and Quantum Gravity **21**, 1 (2004).
[28] M. Calvani, F. de Felice, R. Fabbri, and R. Turolla, Nuovo Cimento B Serie **67**, 1 (1982).
[29] A. R. Prasanna and S. Sengupta, Physics Letters A **193**, 25 (1994).

[30] D. Vokrouhlický and V. Karas, Astronomy and Astrophysics **243**, 165 (1991).
[31] J. Bičák, Z. Stuchlík, and V. Balek, Bulletin of the Astronomical Institutes of Czechoslovakia **40**, 65 (1989).
[32] V. Balek, J. Bičák, and Z. Stuchlík, Bulletin of the Astronomical Institutes of Czechoslovakia **40**, 133 (1989).
[33] Z. Stuchlík, J. Bičák, and V. Balek, General Relativity and Gravitation **31**, 53 (1999).
[34] F. de Felice and F. Sorge, Classical and Quantum Gravity **20**, 469 (2003).
[35] Z. Stuchlík and S. Hledík, Acta Physica Slovaca **48**, 549 (1998).
[36] P. Bakala, E. Šrámková, Z. Stuchlík, and G. Török, Classical and Quantum Gravity **27**, 045001 (2010).
[37] G. Preti, Physical Review D **81**, 024008 (2010).
[38] O. Kopáček, V. Karas, J. Kovář, and Z. Stuchlík, The Astrophysical Journal **722**, 1240 (2010).
[39] J. Kovář, Z. Stuchlík, and V. Karas, Classical and Quantum Gravity **25**, 095011 (2008).
[40] Z. Stuchlík, J. Kovář, and V. Karas, Proceedings of the International Astronomical Union, IAU Symposium **259**, 125 (2009).
[41] J. Kovář, O. Kopáček, V. Karas, and Z. Stuchlík, Classical and Quantum Gravity **27**, 135006 (2010).
[42] F. H. Seguin, The Astrophysical Journal **197**, 745 (1975).
[43] Z. Stuchlík and S. Hledík, Classical and Quantum Gravity **17**, 4541 (2000).
[44] R. M. Wald, *General relativity* (University of Chicago Press, 1984).
[45] K. Avinash, Physics of Plasmas **13**, 012109 (2006).
[46] M. A. Abramowicz, J. C. Miller, and Z. Stuchlík, Physical Review D **47**, 1440 (1993).
[47] T. Neukirch, Astronomy and Astrophysics **274**, 319 (1993).
[48] J. Pétri, J. Heyvaerts, and S. Bonazzola, Astronomy and Astrophysics **384**, 414 (2002).
[49] F. Reif, *Fundamentals of Statistical and Thermal Physics* (Waveland Press, Inc., Nong Grove, IL USA, 1965).